Low Temperature Physics/Fizika Nizkikh Temperatur, 2014, v. 40, No. 3, pp. 259–266

# Excess conductivity analysis and infrared absorption spectroscopy of Mg-doped $TlBa_2Ca_2Cu_3O_{10-\delta}$ superconductor

M. Mumtaz[1,2], M. Zubair[1,2], Nawazish A. Khan[1], and Saleem Abbas[1]

[1] *Materials Science Laboratory, Department of Physics, Quaid-i-Azam University, Islamabad 45320, Pakistan*
E-mail: mmumtaz75@yahoo.com

[2] *Materials Research Laboratory, Department of Physics, FBAS, International Islamic University Islamabad (IIUI) Islamabad 44000, Pakistan*

Received June 6, 2013, revised October 25, 2013

Fluctuation induced conductivity (FIC) analysis on dc resistivity versus temperature data of as-prepared and oxygen post-annealed $TlBa_2(Ca_{2-y}Mg_y)Cu_3O_{10-\delta}$ ($y$ = 0, 0.25, 0.5, 0.75, 1.0) superconductor samples are carried out by using Aslamazov–Larkin model for excess conductivity. The microscopic parameters such as zero temperature coherence length along $c$ axis $\{\xi_c(0)\}$, interlayer coupling ($J$), intergrain coupling ($\alpha$), critical exponent ($\lambda$) and dimensionality of superconducting fluctuations are calculated with the help of aforementioned model. The crossover temperature ($T_o$) is shifted towards higher temperature values with the increase of Mg contents up to $y$ = 0.5 and then start to decrease but still remains greater than those values of undoped samples. The increase in $\xi_c(0)$ and $J$ after Mg-doping at Ca sites shows the improvement of interplane coupling in $TlBa_2(Ca_{2-y}Mg_y)Cu_3O_{10-\delta}$ samples. The appreciable change in all the microscopic parameters extracted from the FIC analysis indicates the optimization of oxygen in all the oxygen post-annealed samples. The increase in relative intensity of almost all the oxygen modes indicates the oxygen diffusion in the unit cell after oxygen post-annealing. The diffusion of oxygen can take place at intergranular sites along with intragranular sites, which increases the grains size, intergrain connectivity and carrier density in $CuO_2$ planes.

PACS: **74.72.–h** Cuprate superconductors;
74.62.Bf Effects of material synthesis, crystal structure, and chemical composition.

Keywords: $TlBa_2(Ca_{2-y}Mg_y)Cu_3O_{10-\delta}$ superconductor, Mg-doping, excess conductivity, post-annealing.

## 1. Introduction

Thallium based high-$T_c$ superconductor family was discovered in 1988 by Sheng and Hermann [1–3]. All of the Tl-based compounds can be described by the general formula $Tl_mA_2Ca_{n-1}Cu_nO_{2n+m+2}$ where $m$ = 1, 2; $n$ = 1, 2, 3, 4, 5; A = Ba, Sr. The compound with $m$ = 1 and $m$ = 2 are usually referred to single and double Tl–O layered compounds, respectively. In double layered thallium-based compounds, $Tl_2Ba_2Cu_1O_6$, $Tl_2Ba_2Ca_1Cu_2O_8$, $Tl_2Ba_2Ca_2Cu_3O_{10}$, $Tl_2Ba_2Ca_3Cu_4O_{12}$, and $Tl_2Ba_2Ca_4Cu_5O_{14}$ are major phases which can be simply represented as Tl-2201, Tl-2212, Tl-2223, Tl-2234, and Tl-2245 with critical temperature of 95, 118, 127, 112, 105 K, respectively [4,5]. These materials exhibit tetragonal symmetry with $P4/mmm$ space group. These compounds can be generally represented by Tl-22($n$ − 1)$n$, where "$n$" represents the number of $CuO_2$ planes. On the other hand, the monolayer Tl-based system includes $TlBa_2Ca_1Cu_2O_7$, $TlBa_2Ca_2Cu_3O_9$, $TlBa_2Ca_3Cu_4O_{11}$, and $TlBa_2Ca_4Cu_5O_{13}$ superconductor phases, which can be represented as Tl-1212, Tl-1223, Tl-1234 and Tl-1245 with critical temperatures 103, 123, 112 and 107 K, respectively [6–14]. The single Tl–O layer compounds have primitive tetragonal structure. The higher superconducting properties of single layer thallium-based compounds make them preferable over double layer thallium-based compounds [9–14].

Almost all the compounds of high-$T_c$ superconducting families have anisotropic behavior in their transport properties due to their layered structures [15–18]. The anisotropic nature promotes fluctuations in the order parameters due to competing effects of different coherence lengths (along $c$ axis and $ab$ plane) during transport processes in these materials. The charge carriers have to tunnel across

the insulating/partially insulating barriers along the $c$ axis and across the grain boundaries during the transport process, which promotes fluctuations in the order parameters. The fluctuations induced conductivity (FIC) analysis is one of the experimentally accessible methods just shedding light on the normal state transport properties of high-$T_c$ oxides. Just above $T_c^{\text{onset}}$, the resistivity $\rho(T)$ is affected by superconducting fluctuations resulting in noticeable deviation of $\rho(T)$ down from its linear dependence at higher temperatures. In the present work, we have tried to unfold the correlation between different microscopic superconductivity parameters of single layer thallium-based Mg-doped $TlBa_2(Ca_{2-y}Mg_y)Cu_3O_{10-\delta}$ ($y$ = 0, 0.25, 0.5, 0.75, 1.0) samples near the transition temperature region. The motivation behind this work is to explore how the insulating charge reservoir layer affects the superconducting properties after interplane coupling by Mg-doping at Ca sites. For this purpose fluctuation induced conductivity has been carried out on dc resistivity versus temperature data. Excess conductivity arises due to superconducting fluctuations [19–23] above the transition temperature in superconductors. There are two models for the polycrystalline samples that can explain the fluctuations in intergrain and intragrain regions. The first model proposed by Aslamasov and Larkin (AL) is associated with fluctuations in intergrain and intragrain regions [23], while the second was developed by Lawrence and Doniach (LD), which can be used only for description of fluctuations in intragrain region [24] of cuprates. The excess conductivity is generally analyzed by using these two models.

According to AL model, the excess conductivity $\Delta\sigma$ is given by

$$\Delta\sigma_{AL} = C\,\varepsilon^{-\lambda}, \tag{1}$$

where $\lambda$ is the critical exponent related to the dimension of superconducting fluctuations and $C$ is the fluctuation amplitude in 2D and 3D regions:

$$C = \frac{e^2}{16\hbar d}, \quad \lambda = 1 \text{ for 2D}, \tag{2}$$

$$C = \frac{e^2}{32\hbar\xi_c(0)}, \quad \lambda = 0.5 \text{ for 3D}, \tag{3}$$

where $e$ is the electronic charge, $\xi_c(0)$ and $d$ are the zero temperature coherence length along the $c$ axis and the interlayer separation, respectively.

The FIC in 2D and 3D regimes can be calculated as

$$\Delta\sigma_{AL} = \frac{e^2}{16\hbar d}\varepsilon^{-1.0} \text{ for 2D}, \tag{4}$$

$$\Delta\sigma_{3D} = \frac{e^2}{32\hbar\xi_c(0)}\varepsilon^{-0.5} \text{ for 3D}. \tag{5}$$

The reduced temperature $\varepsilon$ is given by the relation

$$\varepsilon = \frac{T - T_c^{mf}}{T_c^{mf}}, \tag{6}$$

where $T_c^{mf}$ is the mean field critical temperature and is determined from $\sigma^{-2}$ versus $T$ (K) plot [25]. The dimensional exponent $\lambda$ is found from the slope of $\ln(\Delta\sigma)$ versus $\ln\varepsilon$ plots. It is seen that 2D to 3D crossover is mainly found at a particular temperature ($T_o$) well above the critical temperature, which is different for different samples.

Lawrence–Doniach introduced the concept of interlayer coupling in the neighborhood of the critical temperature via Josephson coupling [24]. According to the LD model for layered superconductors, the excess conductivity $\Delta\sigma_{LD}$ due to superconducting fluctuations is expressed as

$$\Delta\sigma_{LD} = \left(\frac{e^2}{16\hbar d}\right)\varepsilon^{-1}\left[1+\left(\frac{2\xi_c(0)}{d}\right)^2\right], \tag{7}$$

where $\xi_c(0)$ and $d$ are the coherence length along $c$ axis and the interlayer separation, respectively. The LD model predicts that near $T_c$ a crossover of the dimensionality of the fluctuations occurs and is given by

$$T_o = T_c\left[1+\left(\frac{2\xi_c(0)}{d}\right)^2\right]. \tag{8}$$

The second term is the interlayer coupling strength, which is related to the reduced temperature $\varepsilon$ by $J = \varepsilon/4$. The LD model suggests a change from 2D to 3D behavior at $T_o$, which can be determined from the experimental data by extrapolation of straight lines and taking a crossover point.

The excess conductivity induced by superconducting fluctuations is given by

$$\Delta\sigma = \sigma(T) - \sigma_n(T) = 1/\rho(T) - 1/\rho_n(T), \tag{9}$$

where $\rho(T)$ represents experimentally measured resistivity, while $\rho_n(T)$ is the extrapolated resistivity which is calculated by the following equation:

$$\rho_n(T) = \alpha + \beta T, \tag{10}$$

where $\alpha$ is an intercept at 0 K and $\beta$ is a slope of straight line on the normal state resistivity curve.

## 2. Experimental details

The superconducting $TlBa_2(Ca_{2-y}Mg_y)Cu_3O_{10-\delta}$ ($y$ = 0, 0.25, 0.5, 0.75, 1.0) samples were prepared by the solid-state reaction method accomplished in two stages. At the first stage $Ba_2(Ca_{2-y}Be_y)Cu_3O_{10-\delta}$ precursor material was prepared by thoroughly mixing $Ba(NO_3)_2$, $Ca(NO_3)_2$, MgO and Cu(CN) compounds in a quartz mortar and pestle in appropriate ratios. The mixed material loaded in a quartz boat was fired twice at 860 °C for 24 h in a preheated furnace. After 24 h heat treatment, the furnace was switched off and the precursor material was cooled down to room temperature. At the second stage, thallium oxide ($Tl_2O_3$) was mixed with precursor material and was ground for

about an hour. $Tl_2O_3$ mixed material was pelletized under 3.8 tons/cm$^2$ pressure and the pellets were enclosed in gold capsules. The pellets enclosed in gold capsules were sintered at 860 °C for about 10 min and then quenched to room temperature. The samples were characterized by dc-resistivity and ac-susceptibility measurements [26]. The structure of the material was determined by x-ray diffraction (XRD) scan from Rigaku x-ray diffractometer using a Cu$K_\alpha$ source of wavelength 1.54056 Å and the cell parameters were calculated by using the cell refinement computer program. Fourier transform infrared (FTIR) absorption measurements are analyzed to investigate the changes in oxygen phonon modes. FTIR absorption measurements were performed by using a Nickolet TM5700 spectrometer. The spectral resolution was 4 cm$^{-1}$ and 200 scans for the background (KBr) and samples spectra were taken. The post-annealing of the samples in flowing oxygen was carried out in a tubular furnace at 500 °C for 6 h.

### 3. Results and discussion

X-ray diffraction patterns of $TlBa_2(Ca_{2-y}Mg_y)Cu_3O_{10-\delta}$ ($y$ = 0, 0.75) are shown in Fig. 1. Most of the XRD peaks are indexed according to the tetragonal structure following *P4/mmm* space group with cell parameters $a$ = 4.22 Å and $c$ = 15.20 Å for the samples with $y$ = 0 and $a$ = 4.19 Å and $c$ = 15.12 Å for the samples with $y$ = 0.75. The decrease of axes lengths with Mg-doping manifests that the anisotropy of the final compound is decreased [27,28]. The role of phonon modes associated with the various oxygen atoms in the unit cell of cuprates are considered to be highly significant in the mechanism of superconductivity. The FTIR absorption spectra of as-prepared $TlBa_2(Ca_{2-y}Mg_y)Cu_3O_{10-\delta}$ ($y$ = 0, 0.25, 0.5, 0.75, and 1.0) samples are shown in Figs. 2(a), (b). The modes of vibration related to the apical oxygen atoms are observed at around 400–450 cm$^{-1}$, $CuO_2$ planar oxygen atoms around 500–550 cm$^{-1}$ and $O_\delta$ atoms in the $Cu_{0.5}Tl_{0.5}Ba_2O_{4-\delta}$ charge reservoir layer around 600–650 cm$^{-1}$ in CuTl-1223 samples [29,30]. In Mg free Tl-1223 samples, the apical oxygen mode Tl–$O_A$–Cu(2) is observed at around 453 cm$^{-1}$. The $CuO_2$ planar oxygen mode is observed at around 547 cm$^{-1}$ and the $O_\delta$ mode of oxygen in $TlBa_2O_{4-\delta}$ charge reservoir layer is peaked at around 607 cm$^{-1}$. The relative intensities of almost all the oxygen modes have been increased with the increase of Mg content in $TlBa_2(Ca_{2-y}Mg_y)Cu_3O_{10-\delta}$ samples. The increase in the intensity of the $O_\delta$ mode indicates that the oxygen content has been increased with the increase of Mg-doping in $TlBa_2(Ca_{2-y}Mg_y)Cu_3O_{10-\delta}$ samples. The position of apical oxygen mode remains almost the same but the $CuO_2$ planar oxygen mode and $O_\delta$ mode are systematically softened from 547 to 528 cm$^{-1}$ and 607 to 594 cm$^{-1}$ with the increase of Mg-doping, respectively, as shown in Fig. 2(a). The FTIR absorption measurements of oxygen post-annealed $TlBa_2(Ca_{2-y}Mg_y)Cu_3O_{10-\delta}$ samples are shown in

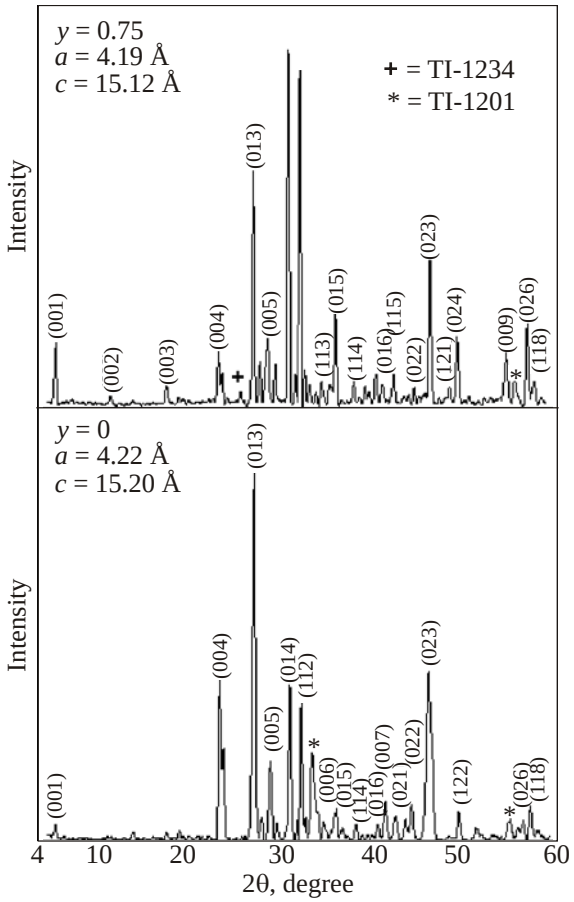


*Fig. 1.* XRD patterns of $TlBa_2(Ca_{2-y}Mg_y)Cu_3O_{10-\delta}$ ($y$ = 0, 0.75) superconductor samples.

Fig. 2(b). The apical oxygen mode Tl–$O_A$–Cu(2) have been observed at around 428–458, 428–460, 429–457, 428–457, and 428–457 cm$^{-1}$, $CuO_2$ planar oxygen modes are observed at around 546, 549, 534, 546, and 536 cm$^{-1}$ and $O_\delta$ mode in the charge reservoir layer are observed at around 596, 591, 577, 570, and 572 cm$^{-1}$ for $y$ = 0, 0.25, 0.5, 0.75, and 1.0, respectively. The apical oxygen modes almost remained at the same positions (i.e., at around 428–457 cm$^{-1}$) but relative intensity has been increased after oxygen post-annealing in all the samples. The increased intensity of almost all the oxygen modes indicates the oxygen diffusion in the unit cell after oxygen post-annealing. The diffusion of oxygen can take place at intergranular sites along with intragranular sites, which increases the grains size, intergrain connectivity and carrier density in $CuO_2$ planes.

The dc electrical resistivity of $TlBa_2(Ca_{2-y}Mg_y)Cu_3O_{10-\delta}$ ($y$ = 0, 0.25, 0.5, 0.75, 1.0) samples was measured using the conventional four-point probe method. The samples were cut in slab form with dimensions of 1.2×1.0×7.0 mm and they were fixed on a sample holder. Four low-electric resistance contacts were made on the samples with silver paint. The fluctuation induced conductivity analysis on the resistivity vs temperature data of $TlBa_2(Ca_{2-y}Mg_y)Cu_3O_{10-\delta}$ samples are carried out by using Aslamazov–Larkin model

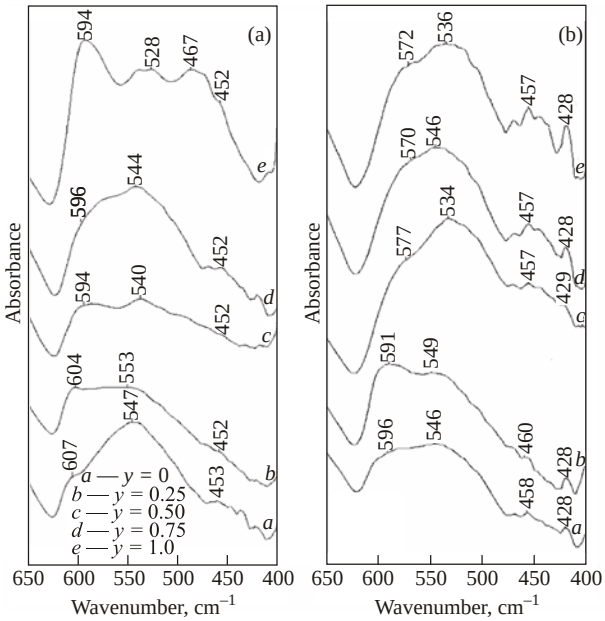


*Fig. 2*. FTIR absorption spectra of $TlBa_2(Ca_{2-y}Mg_y)Cu_3O_{10-\delta}$ ($y$ = 0, 0.25, 0.5, 0.75, and 1.0) superconductor samples: as-prepared (a) and oxygen post-annealed (b).

in the mean field regime. The value of $\lambda_{2D}$ and $\lambda_{3D}$ for as-prepared and oxygen post-annealed samples are given in Tables 1 and 2, respectively. The microscopic parameters such as crossover temperature ($T_o$), mean field critical temperature ($T_c^{mf}$), zero temperature coherence length along $c$ axis {$\xi_c(0)$}, interlayer coupling ($J$) are observed to be improved with the Mg-doping up to $y$ = 0.5 and then slightly decreases but remains greater than those of undoped samples. The decrease in the values is not appreciable. At higher doping level of Mg, it can be expected that Mg may agglomerates at grain-boundaries and causes scattering. Therefore, superconducting properties decrease at higher doping level of Mg in the $TlBa_2Ca_2Cu_3O_{10-\delta}$ superconductor. The decreased value of "α" after oxygen post-annealing shows the improvement of intergrain connectivity in Mg-doped $TlBa_2(Ca_{2-y}Mg_y)Cu_3O_{10-\delta}$ samples. Moreover it is also witnessed that oxygen has been intercalated in our post-annealed samples.

The plots of $\ln(\Delta\sigma_{AL})$ versus $\ln\varepsilon$ of as-prepared $TlBa_2(Ca_{2-y}Mg_y)Cu_3O_{10-\delta}$ samples for $y$ = 0, 0.25, 0.5, 0.75, 0.1 are shown in Fig. 3. In the insets of Fig. 3 are shown the experimentally measured dc resistivity, derivative ($d\rho/dT$) of dc resistivity versus temperature, and the straight line extrapolated from the room temperature (290 K) normal state resistivity to 0 K. The values of $T_c^{mf}$ for the as-prepared samples are determined from the tangent drawn on the $\sigma^{-2}$ versus $T$ curves, Fig. 3(f). The fitting of experimental curves shows the existence of two different fluctuation regions in these samples. The values of critical exponent (λ) derived from the slopes of sample with $y$ = 0 is found to be 0.51 and 1.08, which correspond to 3D and 2D AL fluctuations, respectively. Also, the value of λ were found to be (0.49, 1.09), (0.5, 1.05), (0.49, 1.14) and (0.52, 1.03) with $y$ = 0.25, 0.5, 0.75, and $y$ = 1.0, respectively, for 3D and 2D fluctuations. There is a crossover temperature at which fluctuations have been changed from 2D to 3D in low-temperature region. The plots of $\ln(\Delta\sigma_{AL})$ versus $\ln\varepsilon$

Table 1. The superconductivity parameters observed from the FIC analysis of as-prepared $TlBa_2(Ca_{2-y}Mg_y)Cu_3O_{10-\delta}$ ($y$ = 0, 0.25, 0.5, 0.75, 1.0) superconductor samples

| Sample | $\rho_n$(290 K), Ω·cm | $T_c$, K | $T_o$, K | $T_c^{mf}$, K | $\alpha = \rho_n$(0K), Ω·cm | $\lambda_{3D}$ slope | $\lambda_{2D}$ slope | $\xi_c(0)$, Å | $J = [2\xi_c(0)]^2/d^2$ |
|---|---|---|---|---|---|---|---|---|---|
| $y$ = 0 | 0.031 | 102 | 107.37 | 104.10 | 0.0067 | 0.51 | 1.08 | 1.712 | 0.052 |
| $y$ = 0.25 | 0.014 | 106 | 111.38 | 107.9 | 0.0113 | 0.49 | 1.09 | 1.689 | 0.050 |
| $y$ = 0.5 | 0.012 | 115 | 135.52 | 116.53 | 0.0063 | 0.5 | 1.05 | 3.244 | 0.187 |
| $y$ = 0.75 | 0.040 | 103 | 108.37 | 104.68 | 0.0094 | 0.49 | 1.14 | 1.704 | 0.051 |
| $y$ = 1.0 | 0.031 | 101 | 111.38 | 103.37 | 0.0149 | 0.52 | 1.03 | 2.397 | 0.102 |

Table 2. The superconductivity parameters observed from the FIC analysis of oxygen post-annealed $TlBa_2(Ca_{2-y}Mg_y)Cu_3O_{10-\delta}$ ($y$ = 0, 0.25, 0.5, 0.75, 1.0) superconductor samples

| Sample | $\rho_n$(290 K), Ω·cm | $T_c$, K | $T_o$, K | $T_c^{mf}$, K | $\alpha = \rho_n$(0K), Ω·cm | $\lambda_{3D}$ slope | $\lambda_{2D}$ slope | $\xi_c(0)$, Å | $J = [2\xi_c(0)]^2/d^2$ |
|---|---|---|---|---|---|---|---|---|---|
| $y$ = 0 | 0.0679 | 102 | 106.36 | 103.18 | 0.0173 | 0.5 | 1.4 | 1.719 | 0.0525 |
| $y$ = 0.25 | 0.0158 | 116 | 132.45 | 117.78 | 0.0135 | 0.52 | 0.77 | 2.911 | 0.1507 |
| $y$ = 0.5 | 0.0499 | 111 | 116.40 | 113.23 | 0.0048 | 0.5 | 1.55 | 1.753 | 0.0546 |
| $y$ = 0.75 | 0.0713 | 97 | 101.34 | 99.07 | 0.024 | 0.51 | 1.14 | 2.528 | 0.1136 |
| $y$ = 1.0 | 0.0432 | 108 | 113.91 | 109.98 | 0.0136 | 0.49 | 1.1 | 1.6081 | 0.0459 |

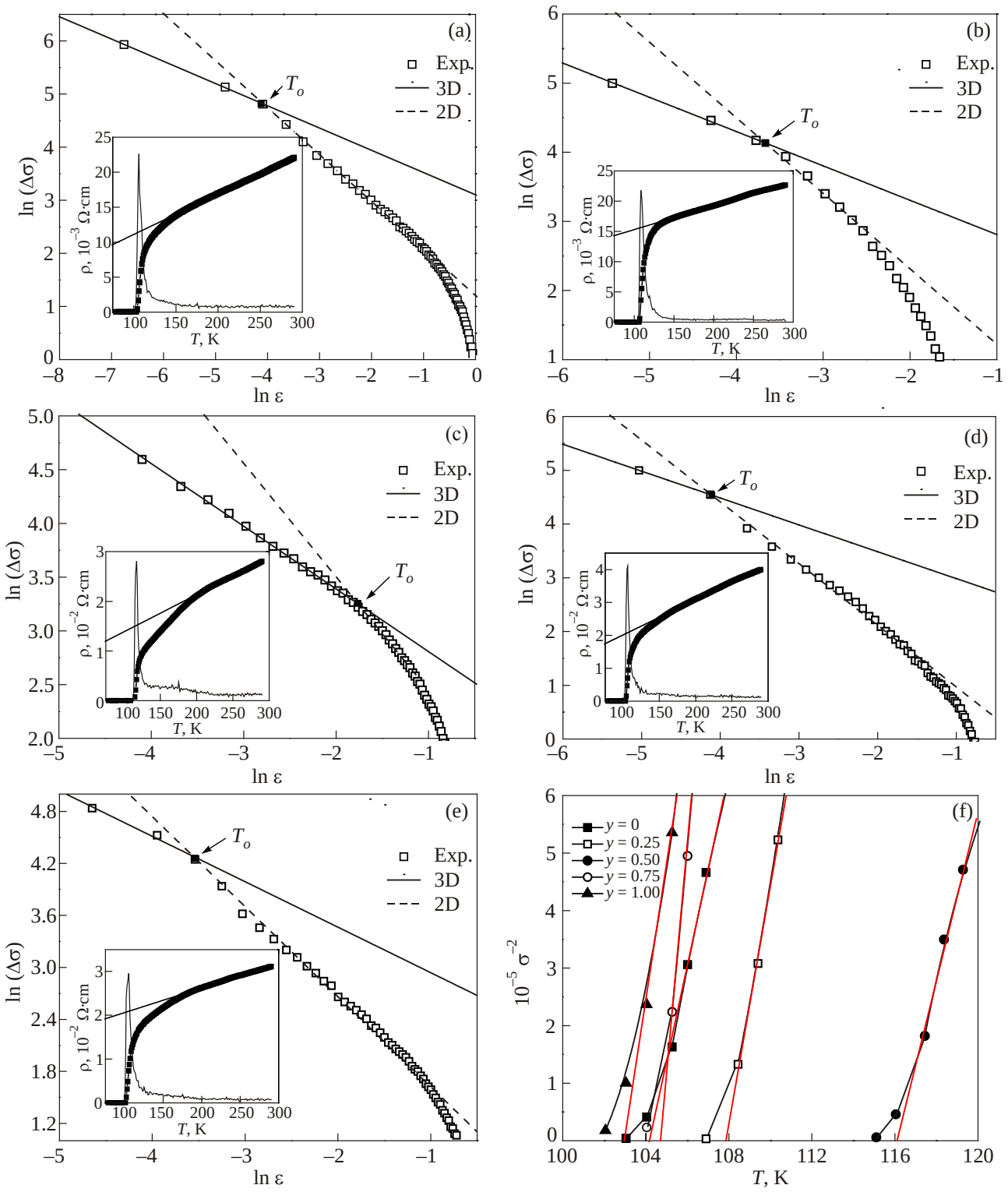


*Fig. 3.* ln (Δσ) versus ln ε plot of as-prepared $TlBa_2Ca_{2-y}Mg_y Cu_3O_{10-\delta}$ samples: $y$ = 0 (a), 0.25 (b), 0.5 (c), 0.75 (d), 0.1 (e). (In the insets are shown the experimentally measured dc resistivity ρ(Ω·cm), derivative ($d\rho/dT$) of dc resistivity versus temperature, and the straight line extrapolated from the room temperature (300 K) normal state resistivity to 0 K). The tangent drawn on the $\sigma^{-2}$ versus $T$ (K) curves of as-prepared $TlBa_2(Ca_{2-y}Mg_y)Cu_3O_{10-\delta}$ ($y$ = 0, 0.25, 0.5, 0.75, and 1.0) superconductor samples (f).

of oxygen-post annealed $TlBa_2(Ca_{2-y}Mg_y)Cu_3O_{10-\delta}$ samples for $y$ = 0, 0.25, 0.5, 0.75, 0.1 are shown in Fig. 4. Also in the insets of Fig. 4 are given the experimentally measured resistivity, derivative of dc resistivity versus temperature, and the straight line extrapolated from the room temperature (290 K) normal state resistivity to 0 K. The values of $T_c^{mf}$ for the oxygen-post annealed samples are determined from the tangent drawn on the $\sigma^{-2}$ versus $T$ curves,

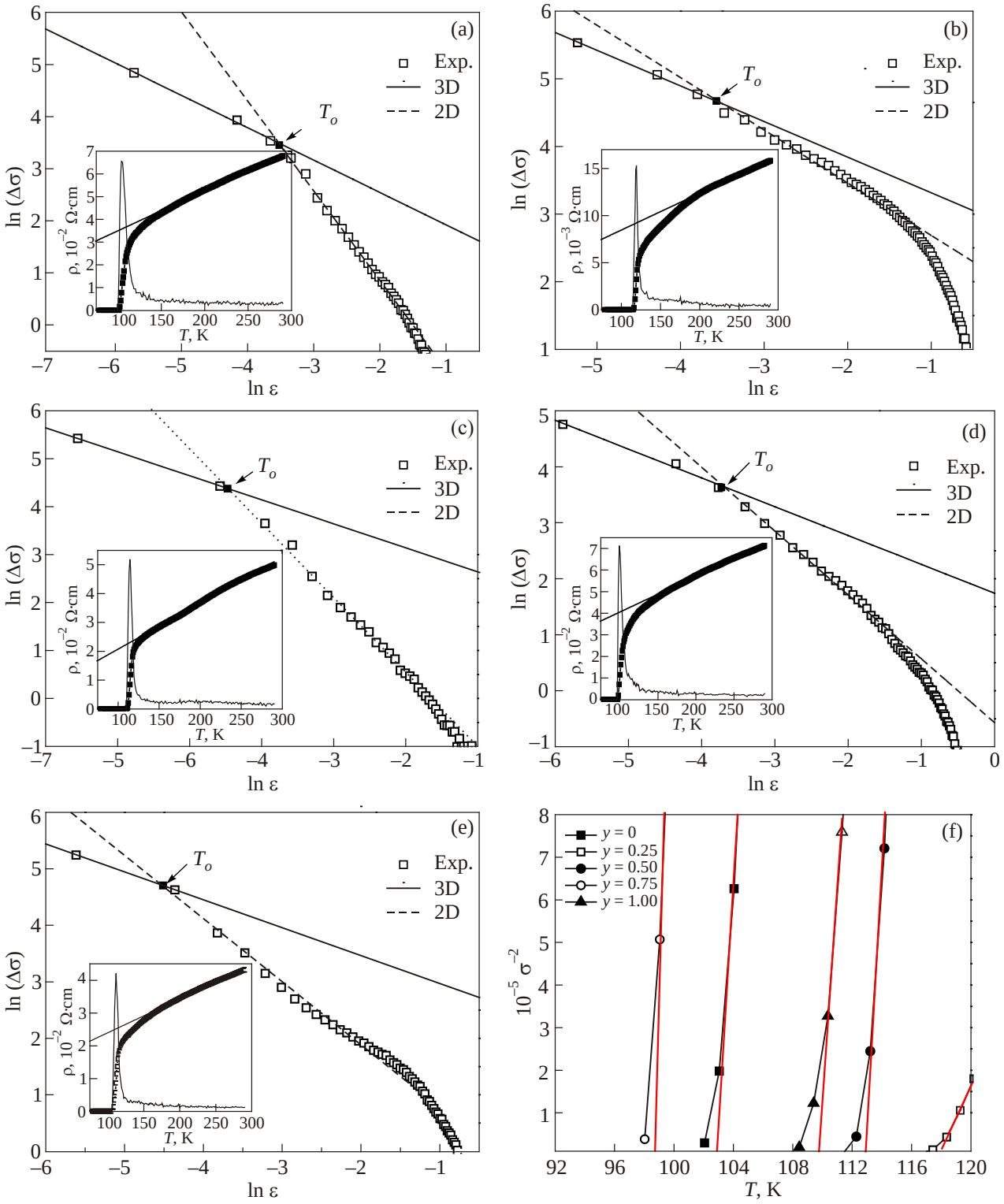


*Fig. 4.* ln (Δσ) versus ln ε plot of oxygen post-annealed $TlBa_2Ca_{2-y}Mg_y Cu_3O_{10-\delta}$ samples: $y$ = 0 (a), 0.25 (b), 0.5 (c), 0.75 (d), 0.1 (e). (In the insets are shown the experimentally measured dc resistivity ρ(Ω·cm), derivative ($d\rho/dT$) of dc resistivity versus temperature, and the straight line extrapolated from the room temperature (300 K) normal state resistivity to 0 K). The tangent drawn on the $\sigma^{-2}$ versus $T$ (K) curves of oxygen post-annealed $TlBa_2(Ca_{2-y}Mg_y)Cu_3O_{10-\delta}$ ($y$ = 0, 0.25, 0.5, 0.75, and 1.0) superconductor samples (f).

Fig. 4(f). The values of λ deduced from the slopes are found to be (0.5, 1.4), (0.52, 0.77), (0.5, 1.55), (0.5, 1.14) and (0.49, 1.1) for $y$ = 0.25, 0.5, 0.75, and 1.0, respectively, corresponding to 3D and 2D fluctuations.

The microscopic parameters such as crossover temperature ($T_o$), zero resistivity critical temperature ($T_c$), coherence length along $c$ axis ($\xi_c$) and coupling constant ($J$) extracted from the fitting of excess conductivity data of as-

prepared and oxygen post-annealed samples are given in Tables 1 and 2, respectively. The widths of these fluctuation regions are given in Tables 3 and 4. It can be seen from the data that $T_o$ has been shifted toward higher temperature with Mg-doping. On the other hand, $\{\xi_c(0)\}$ and $J$ have been improved with Mg-doping, which show that interlayer coupling is increased in these samples. The improvement in the value of $\xi_c$ makes us to conclude that our samples become more isotropic with Mg-doping as compared to undoped samples.

The values of the critical exponent ($\lambda_{3D}$) for as-prepared samples are 0.51, 0.49, 0.5, 0.49 and 0.52 in the temperature regime of 105.36–107.37, 108.37–110.38, 118.46–135.52, 105.36–106.36 and 104.35–106.36, respectively, as given in Table 3, while for oxygen post-annealed samples are 0.5, 0.52, 0.5, 0.5 and 0.49 in the temperature range of 103.35–105.36, 118.40–120.41, 113.31–114.39, 99.34–101.34 and 110.38–111.38, respectively, as given in Table 4. The shift of 3D regime to higher temperature indicates that Mg-doping increases the grain size resulting in the improvement of $T_c$ and $T_o$. The values of the critical exponent ($\lambda_{2D}$) for as-prepared samples are 1.08, 1.09, 1.05, 1.14 and 1.03 in the temperature regime of 107.37–138.47, 111.38–116.40, 135.52–154.60, 106.36–129.44 and 106.36–147.50, respectively, while for oxygen post-annealed samples are 1.4, 0.77, 1.55, 1.14 and 1.1 in the temperature regime of 105.36–135.46, 120.41–154.53, 114.39–129.44, 101.34–124.42, 111.38–147.50, respectively.

The superconductivity has been increased due to improved interplane coupling by the substitution of Mg at Ca sites in between the $CuO_2$ planes and oxygen post-annealing experiments are carried out for further improvement of superconducting properties of $TlBa_2(Ca_{2-y}Mg_y)Cu_3O_{10-\delta}$ samples.

## 4. Conclusions

A series of superconducting $TlBa_2(Ca_{2-y}Mg_y)Cu_3O_{10-\delta}$ ($y$ = 0, 0.25, 0.5, 0.75, 1.0) samples were successfully synthesized by solid state reaction method. The excess conductivity $\Delta\sigma$ derived from the dc resistivity measured data to be fitted very well with 3D and 2D Aslamasov–Larkin equations. The crossover temperature ($T_o$) is shifted towards higher temperature values with the increased Mg-doping concentration up to $y$ = 0.5 and then slightly decreases but remains greater than those of undoped samples. The width of the temperature window in 3D conductivity is increased with the incorporation of Mg in almost all as-prepared samples. The increase in the value of $\xi_c$ and $J$ with Mg-doping indicates that these samples become less anisotropic and interlayer coupling has been improved. The value of $\alpha$ has been decreased after oxygen post-annealing with the increase of Mg-content, which showed that intergrain coupling has been further improved. The appreciable change in all the microscopic parameters extracted from the FIC analysis verifies the oxygen incorporation in all post-annealed samples. The increase in relative intensity of almost all the oxygen modes indicates the oxygen

Table 3. Widths of critical 3D and 2D fluctuation regions observed from fitting of the experimental data of as-prepared $TlBa_2(Ca_{2-y}Mg_y)Cu_3O_{10-\delta}$ ($y$ = 0, 0.25, 0.5, 0.75, 1.0) samples using AL model

| Sample | $\lambda_{3D}$ $T$, K | ln ε (range in 3D) | $\lambda_{2D}$ $T$, K | ln ε (range in 2D) |
|---|---|---|---|---|
| $y$ = 0 | 105.36–107.37 | –4.4 < ln ε < –3.46 | 107.37–138.47 | –3.46 < ln ε < –1.07 |
| $y$ = 0.25 | 108.37–110.38 | –5.4 < ln ε < –3.77 | 111.38–116.40 | –3.77 < ln ε < –2.54 |
| $y$ = 0.5 | 118.46–135.52 | –4.0 < ln ε < –1.81 | 135.52–154.60 | –1.81 < ln ε < –1.11 |
| $y$ = 0.75 | 105.36–106.36 | –5.03 < ln ε < –4.12 | 106.36–129.44 | –4.12 < ln ε < –1.44 |
| $y$ = 1.0 | 104.35–106.36 | –4.6 < ln ε < –3.54 | 106.36–147.50 | –3.54 < ln ε < –0.85 |

Table 4. Widths of critical 3D and 2D fluctuation regions observed from fitting of the experimental data of oxygen post-annealed $TlBa_2(Ca_{2-y}Mg_y)Cu_3O_{10-\delta}$ ($y$ = 0, 0.25, 0.5, 0.75, 1.0) samples using AL model

| Sample | $\lambda_{3D}$ $T$, K | ln ε (range in 3D) | $\lambda_{2D}$ $T$, K | ln ε (range in 2D) |
|---|---|---|---|---|
| $y$ = 0 | 103.35–105.36 | –6.37 < ln ε < –3.85 | 105.36–135.46 | –3.85 < ln ε < –1.16 |
| $y$ = 0.25 | 118.40–120.41 | –5.23 < ln ε < –3.79 | 120.41–154.53 | –3.79 < ln ε < –1.16 |
| $y$ = 0.5 | 113.31–114.39 | –6.55 < ln ε < –4.57 | 114.39–129.44 | –4.57 < ln ε < –1.94 |
| $y$ = 0.75 | 99.34–101.34 | –5.89 < ln ε < –3.77 | 101.34–124.42 | –3.77 < ln ε < –1.36 |
| $y$ = 1.0 | 110.38–111.38 | –5.61 < ln ε < –4.36 | 111.38–147.50 | –4.36 < ln ε < –1.05 |

diffusion in the unit cell after oxygen post-annealing the samples. The diffusion of oxygen can take place at intergranular sites along with intragranular sites, which increases the grains size, intergrain connectivity and carrier density in $CuO_2$ planes and all these factors play the significant role in improving the superconducting properties of the material.


1. Z.Z. Sheng and A.M. Hermann, *Nature* **332**, 55 (1988).
2. Z.Z. Sheng, A.M. Hermann, A.E. Ali, C. Almasan, J. Estrada, T. Datta, and R.J. Matson, *Phys. Rev. Lett.* **60**, 937 (1988).
3. Z.Z. Sheng and A.M. Hermann, *Nature* **332**, 138 (1988).
4. C. Martin, C. Michel, A. Maignan, M. Hervieu, and B. Raveau, *C.R. Acad. Sci. Ser.* 2, **307**, 27 (1988).
5. C. Park and R.L. Synder, *J. Am. Ceram. Soc.* **78**, 3171 (1995).
6. A. Sundaresan, H. Asada, A. Crisan, J.C. Nie, H. Kito, A. Iyo, Y. Tanaka, M. Kusunoki, and S. Ohshima, *IEEE Trans. Appl. Supercond.* **13**, 2913 (2003).
7. J.Y. Juang, J.H. Horng, S.P. Chen, C.M. Fu, K.H. Wu, T.M. Uen, and Y.S. Gou, *Appl. Phys. Lett.* **60**, 885 (1995).
8. A. Sundaresan, H. Asada, A. Crisan, J.C. Nie, H. Kito, A. Iyo, T. Tanaka, M. Kusunoki, and S. Oshima, *Physica C* **388**, 473 (2003).
9. D.J. Miller, J.G. Hu, J.D. Hettinger, K.E. Gray, J.E. Tkaczyk, J. Deluca, P.L. Karas, J.A. Sutliff, and M.F. Garauskas, *Appl. Phys. Lett.* **63**, 556 (1993).
10. A. Iyo, Y. Ishiura, Y. Tanaka, P. Badica, K. Tokiwa, T. Watanabe, and H. Ihara, *Physica C* **370**, 205 (2002).
11. W. Mexner, J. Hoffmann, S. Heede, K. Heinemann, H.C. Freyhardt, F. Ladenberger, and E. Schwarzmann, *Z. Phys. B* **101**, 181 (1996).
12. D.N. Zheng, J.D. Johnson, A.R. Jones, A.M. Campbell, W.Y. Liang, T. Doi, M. Okada, and K. Higashyama, *J. Appl. Phys.* **77**, 5287 (1995).
13. R.T. Liu, S.L. Yan, L. Fang, and M. He, *Supercond. Sci. Technol.* **14**, 948 (2001).
14. R.S. Liu, D.N. Zheng, J.W. Loram, K.A. Mirza, A.M. Campbell, and P.P. Edwards, *Appl. Phys. Lett.* **60**, 1019 (1992).
15. E.F. Talantsev, N.M. Strickland, P. Hoefakker, J.A. Xia, and N.J. Long, *Current Appl. Phys.* **8**, 388 (2008).
16. E. Giannini, R. Gladyshevskii, N. Clayton, N. Musolino, V. Garnier, A. Piriou, and R. Flükiger, *Current Appl. Phys.* **8**, 115 (2008).
17. E. Aksu, A. Gencer, N. Calinli, H. Koralay, and S. Cavdar, *Physica C* **363**, 158 (2005).
18. P. Badica, T. Kondo, K. Togano, and K. Yamada, *J. Phys. Chem. Solids* **67**, 590 (2006).
19. Han-Yong Choi, Yunkyu Bang, and David K. Campbell, *Phys. Rev. B* **61**, 9748 (2000).
20. K. Nakayama, T. Sato, Y. Sekiba, K. Terashima, P. Richard, T. Takahashi, K. Kudo, N. Okumura, T. Sasaki, and N. Kobayashi, *Phys. Rev. Lett.* **102**, 227006 (2009).
21. A.N. Artemov and A.Yu. Martynovich, *Fiz. Nizk. Temp.* **22**, 638 (1996) [*Low Temp. Phys.* **22**, 488 (1996)].
22. Rui-Hua He, M. Hashimoto, H. Karapetyan, J.D. Koralek, J.P. Hinton, J.P. Testaud, V. Nathan, Y. Yoshida, Hong Yao, K. Tanaka, W. Meevasana, R.G. Moore, D.H. Lu, S.-K. Mo, M. Ishikado, H. Eisaki, Z. Hussain, T.P. Devereaux, S.A. Kivelson, J. Orenstein, A. Kapitulnik, and Z.-X. Shen, *Science* **331**, 1579 (2011).
23. L.G. Aslamasov and A.I. Larkin, *Phys. Lett. A* **26**, 238 (1968).
24. W.E. Lawrence and S. Doniach, *Proceed. 12th Int. Conf. on Low Temperature Physics*, Kyoto, Japan, E. Kanda (ed.), Keigaku, Tokyo (1971), p. 361.
25. B. Oh, K. Char, A.D. Kent, M. Naito, M.R. Beasley, T.H. Geballe, R.H. Hammond, and A. Kapitulink, *Phys. Rev. B* **13**, 37 (1988).
26. Nawazish A. Khan, M. Zubair, M. Mumtaz, and A.A. Khurram, *Ceramics Intern.* **39**, 1901 (2013).
27. Nawazish A. Khan and A.A. Khurram, *Appl. Phys. Lett.* **86**, 152502 (2005).
28. Nawazish A. Khan and M. Mumtaz, *Matter Lett.* **62**, 659 (2008).
29. A.D. Kulkarni, J. Prade, and F.W. de Wette, *Phys. Rev. B* **40**, 2642 (1989).
30. A.D. Kulkarni, F.W. de Wette, J. Prade, U. Schroder, and W. Kress, *Phys. Rev. B* **41**, 6409 (1990).